Gurubaran et al. 2017. *Int. J. Vehicle Structures & Systems*, 9(3), 186-189
ISSN: 0975-3060 (Print), 0975-3540 (Online)
doi: 10.4273/ijvss.9.3.11

International Journal of Vehicle Structures & Systems
Available online at www.maftree.org/eja

Three Dimensional Finite Element Analysis of Rolling Contact between Wheel and Rail

P. Gurubaran[a,c], M. Afendi[a,e], I. Haftirman[b] and K. Nanthini[c]

[a]*School of Mechatronic Engg., Universiti Malaysia Perlis, Malaysia*
[b]*University Mercu Buana, Kampus Menara Bakti Fakultas Teknik, Jakarta Barat, Indonesia*
[c]*Faculty of Mech. and Mfg., Universiti Tun Hussein Onn Malaysia, Johor, Malaysia*
[d]*Corresponding Author, Email: gurubaranpanerselvan@gmail.com*
[e]*Email: afendirojan@unimap.edu.my*

ABSTRACT:

The fatigue performance of the rails is affected by many factors, including service conditions, loading, mechanical properties, environment factors, and manufacturing processes. In this paper, the investigation on wheel-rail to identify the initial damages caused by Rolling Contact Fatigue (RCF) cracks and the location that experienced damages is presented. UIC 54kg rail (grade 900A) was used as the model in three dimensional (3D) finite element contact analysis. The fatigue crack growth on wheel-rail was carried out by considering the Hertz contact pressure. The finite element analysis results show that maximum stress concentration zone was between the wheel-rail surface (rail inside curve gauge corner) and it is above the yield stress limit for wheel-rail steel. Fatigue crack propagation within a depth affected stress concentration region was predicted. The stress intensity factors (SIF) for mode I, mode II and mode III fracture were plotted from ANSYS simulation. Three types of fracture modes were affected the UIC54kg rail Steel to fail or develop initial failure when the crack propagation exceeds 5 mm.

KEYWORDS:

Rolling contact fatigue; Finite element analysis; Rail-wheel crack initiation; Stress intensity factor; Crack growth

CITATION:

P. Gurubaran, M. Afendi, I. Haftirman and K. Nanthini. 2017. Three Dimensional Finite Element Analysis of Rolling Contact between Wheel and Rail, *Int. J. Vehicle Structures & Systems*, 9(3), 186-189. doi:10.4273/ijvss.9.3.11.

1. Introduction

The Rolling Contact Fatigue (RCF) in rail is caused by the wheel-rail contact which leads initiation of surface and subsurface cracks [1]. The fatigue performance of the rails is affected by many factors, including service conditions, loading, mechanical properties, environment factors, and manufacturing processes [2]. Contact fatigue is defined as damage due to change in the material microstructure which contributes to crack initiation followed by crack propagation, under the influence of time-dependent rolling and sliding contact loads. There is a close relationship between the wear and contact fatigue at wheel-rail [3]. If the crack growth rate is higher than wear, it causes the crack to develop faster leading to sudden rail failure. Fatigue is the major type of material degradation failure between the wheel and rail contact load [4]. Material degradation damage that is caused by the accumulation of material microstructure can occur with repeated rolling and slide. The life of a fatigue crack is divided into three phases [5]. In phase I, the shear stress is applied to the surface which initiates the crack, phase II is the transient crack growth behaviour and phase III is the subsequent tensile and shear driven crack growth.

RCF analysis involves fatigue crack initiation and fatigue crack propagation. In order to investigate the fatigue crack initiation, 3D finite element analysis (FEA) was conducted by applying the contact stress based on Hertz theory [5]. For the study of fatigue crack growth on wheel-rail, 3D finite element analysis was carried out by considering the Hertz contact pressure. The analysis was extended to mixed mode crack growth study in the wheel-rail contact region based on strain energy release rate [3]. In this paper, the investigation was based upon the failure sample that provided by Malaysia Railways as shown in Fig. 1. The main aim is to identify the initial damages caused by fatigue and the location that mostly faced the damages.

Fig. 1: Fatigue failure rail sample to identify initial damage development (UIC 54kg)

According to failure sample in Fig. 1, the formation and three stages growth of head check were identified from the previous study [6]. The crack initiation stage at the surface of rail called as stage I, followed by stage II where the crack growth at a shallow angle of the rail, and in stage III where the head check growth is increased in the crack propagation at the rail head region. This head check is also called as superficial (surface) cracks at the surface of the rail, and commonly this may change to transverse crack after propagation because of many factors such as loading, friction, and initial rail gauge corner crack. The transverse crack should be noted because it is one of the dangerous cracks in rails [4]. Fatigue crack growth forms crack branching along the direction of plastic deformation [7]. The development of head check was based on cyclic, plastic deformation of the rail Steel that results from the shear and compressive stress acting between the wheel-rail contact zone areas [6]. The high stress between the wheel and rail results in plastic deformation at the running surface on the wheel and the rails [8]. Rajasekaran et al studied the mesh model quality and its convergence criteria for quality mesh flow in the FE models [9].

2. Materials and methods

In order to construct the geometric modelling of wheel and rail, the prominent profile in Malaysia Railways named as UIC 54kg rail was used as the material in finite element contact analysis. The analysis was performed by using ANSYS to investigate the rolling contact fatigue between the rail and wheel which can lead to total failure of railways. The 3D FEA and simulation were performed to specify the location of maximum stress field due to wheel-rail contact by considering all possible parameters in Malaysia railways system. Further, the 3D model geometry that has been created from Catia was transferred to the ANSYS 14.5 (work bench) and assembled on half symmetry model consisting of wheel and rail as presented in Fig. 2. The half symmetry cross-sectional area of rail was a model for observing the maximum load distribution between the rail and wheel more clearly as shown in Fig. 4. Fig. 3 shows the image of rail inside curve which is the rail contact region between the wheel and the most common area of head check damage occurrence.

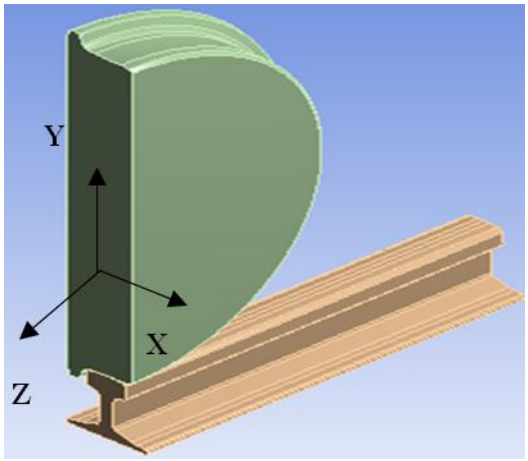

Fig. 2: Wheel and rail model in static loading condition using ANSYS FEA

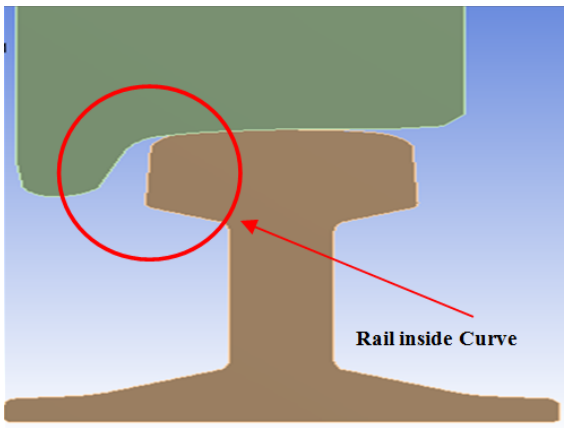

Fig. 3: Modeling of wheel-rail at contact (rail inside curve)

The lateral load for the analysis was neglected due to actual flat and straight path. The effect on the wheel rotation was also ignored. The mechanical properties for wheel-rail UIC54 kg (grade 900A) are presented in Table 1. The wheel-rail model was meshed with SOLID 45 8-noded hex, and equivalent Von Mises stress analysis was carried out with static condition using 3D linear elastic-plastic finite element model. The contact between the wheel and rail was modelled with contact173 and target170 elements respectively. The wheel-rail linear material density is 7.850(g/cc) and friction coefficient is defined as 3.0 (constant) for all directions. The vertical load for wheel-rail contact was applied as 6000N per wheel. Only half of rail was modelled because of longitudinal symmetry. The total vertical load was applied at shaft location to represent no approximation of load transfer between the wheel-rail contacts. The stress intensity factors (SIF) for mode I (K_I - Opening mode), mode II (K_{II} - Mixed mode)and mode III (K_{III} - Shearing mode) fracture were evaluated by obtaining the maximum Von Mises stress between the wheel and rail. The SIF was computed using ANSYS 14.5 and at the static contact point of wheel-rail. The study of SIF was improved by modeling a contour line along the wheel and rail contact region. The contours along the motion and load movement as shown in Fig. 4 are considered. This loading is associated with the train weight that acts perpendicular to the rail.

Table 1: Properties for wheel and rail - UIC54 kg (grade 900A) [9]

Parameter	Value
Ultimate strength (MPa)	924
Yield strength (MPa)	533
Strain hardening exponents (n)	0.243
Poisson ratio	0.3
Elongation of fracture (%)	12

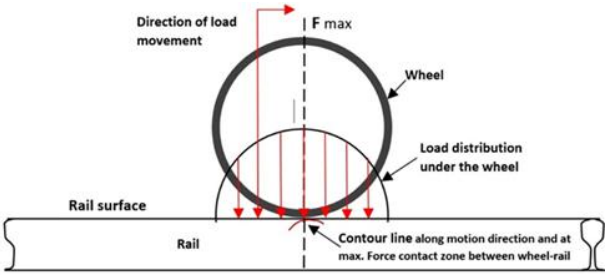

Fig. 4: Definition of loading condition and contour line between wheel-rail contact regions

3. Results and Discussion

The numerical simulation was further investigated on half symmetry cross-sectional area of the wheel and rail model. In Fig. 5, the Von Mises stress distribution was presented for both wheel and rail for applied static force. The Von Mises stress gradient at rail shallow angle result was presented in Fig. 6. As expected the maximum stress concentration value showed high at rail gauge corner region. Based on this simulation result, it can be concluded that the UIC54kg (grade 900A) rail Steel started to fail due to plastic deformation present at rail inside curve region and compromising the rail structural integrity. The maximum Von Mises stress of 870.11 MPa was obtained for rail inside curve region which is greater than 533 MPa yield stress limit for the wheel-rail Steel. In comparison to the previous study done by the author [1] revealed that the similar result where the maximum stress zone concentration between the wheel-rail exceeded the yield stress limit of Steel at the rail inside curve region. The equivalent plastic stress result shown in Fig. 6 reveals that most of the plastic deformation occurs at the rail than at the wheel. The initial damage was developed on the failure sample due to a maximum load of wheel profile contact towards the rail gauge corner (red box). The damage was occurred due to the high concentration of stress at rail inside curve region which exceeds the yield stress limit of rail steel. From this investigation, the initial rail gauge corner growth at failure sample was contributed towards developing critical rail head check damage (blue box) as shown in Fig. 7.

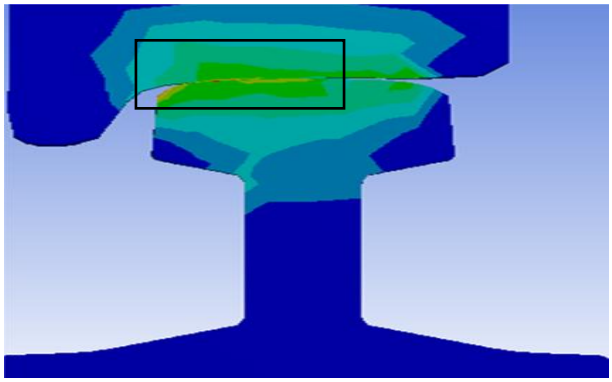

Fig. 5: Von Mises stress gradient between rail and wheel in contact

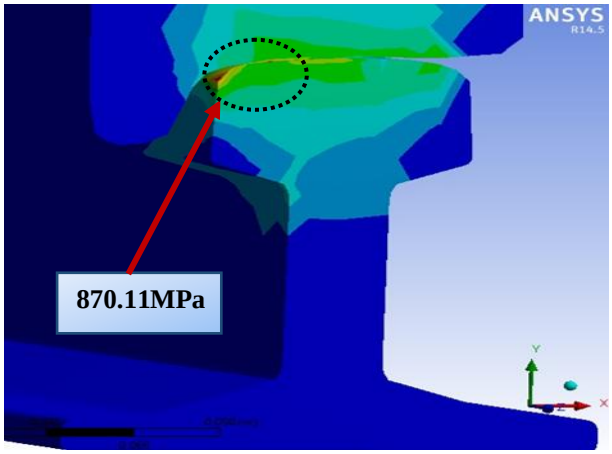

Fig. 6: Plastic deformation at rail inside curve (rail gauge corner)

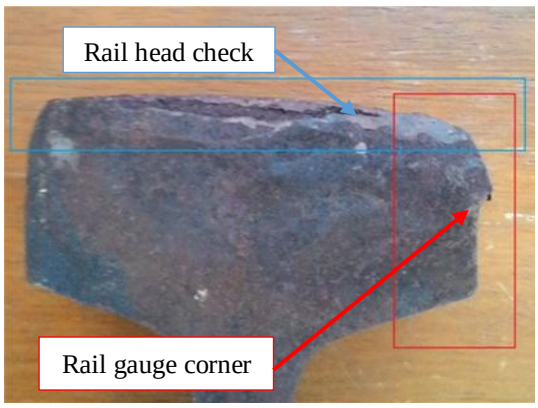

Fig. 7: Damage location on rail inside curve sample

In addition, the damage was occurred due to the Hertz contact pressure which was applied on the rolling contact between the rail and wheel. From the overall findings, the maximum stress at the rail inside curve, distributed to the centre of rail head for every contact between rail-wheel. This has contributed towards developing head check damage at rail head. Therefore, the plastic deformation was formed due to the stress contact exceeding the rail Steel yield limit. This contributed to fatigue crack growth with crack branching along the surface on the rail head. Figs. 8-10 show the stress intensity factors for mode I, mode II, and mode III fracture which were plotted from ANSYS simulation.

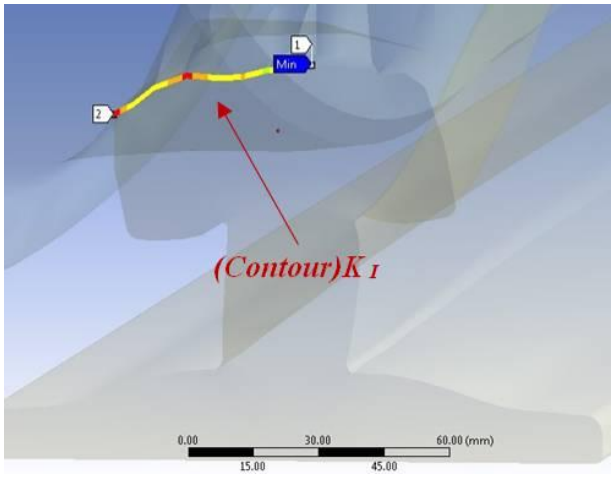

Fig. 8: Mode I (opening mode SIF) contour between rail and wheel

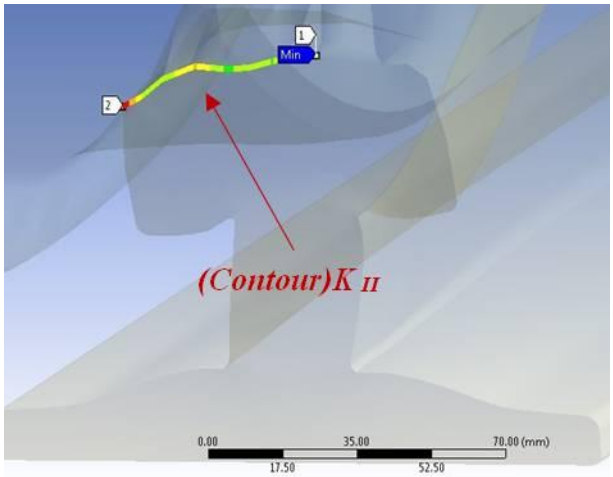

Fig. 9: Mode II (mixed mode SIF) contour between rail and wheel

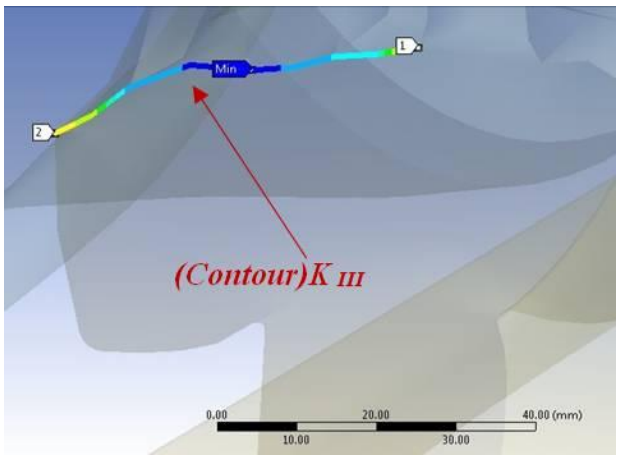

Fig. 10: Mode III (shearing SIF) contour between rail & wheel

The SIF analysis was conducted between the wheel-rail contact regions to investigate the fatigue crack growth propagation and capability of UIC54 kg (grade 900A) rail Steel to resist the crack. For that purpose, 10mm contour lines were modelled along maximum Von Mises stress contact regions. The value obtained for SIF from ANSYS simulation was not consistent due to non-proportional strain energy release rate. Fig. 11 shows the simulation SIF result for the railway material. The capability to resist the cracks for mode I is K_I = 0.4 MPa, mode II is K_{II} = 0.21MPa and mode III is K_{III} = -0.9 MPa. Based on the result in Fig. 11, the railway material has failed and started to damage the rail inside curve region once the SIF exceeded 5mm of crack for all 3 types of fracture mode. The difference in value obtained for K_{III} results in Fig. 11 is due to change in the crack path direction and changes in the driving force between three modes of fracture.

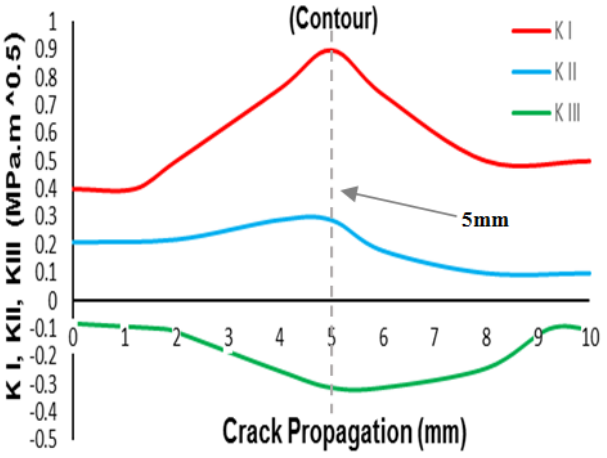

Fig. 11: SIF along the motion direction for railway grade 900A material (modes I - III)

4. Conclusion

The numerical analysis stress characteristic of wheel-rail contact was successfully carried out using 3D FEA. The results are observed as very helpful in visualizing and identifying the initial damage growth from the rail gauge corner to head check damage. Wheel-rail stress concentration exceeded the yield stress limit of wheel-rail Steel. The increase of stress field in the wheel-rail contact zone is the most important in fatigue life reduction leading a sudden failure. From the rail gauge corner, the stress is distributed to the centre of rail head for every contact between the wheel-rail and this has developed head check damage at rail head. Initial high stress concentration at rail inside curve region has contributed to rail damage by maximum contact stress at head check. The stress intensity factor investigation showed that three modes of fracture determine the capability of railway's material to withstand damages.

REFERENCES:

[1] R.M. Nejad, M. Shariati and K. Farhangdoost. 2016. Effect of wear on rolling contact fatigue crack growth in rails, *Tribology Int.*, 94, 118-125. http://dx.doi.org/10.1016/j.triboint.2015.08.035.

[2] G. Fajdiga and M. Sraml. 2009. Fatigue crack initiation and propagation under cyclic contact loading, *Engg. Fracture Mech.*, 76(9), 1320-1335. http://dx.doi.org/10.1016/j.engfracmech.2009.02.005.

[3] Y. Liu, L. Liu and S. Mahadevan. 2007. Analysis of subsurface crack propagation under rolling contact loading in railroad wheels using FEM, *Engg. Fracture Mechanics*, 74(17), 2659-2674. http://dx.doi.org/10.1016/j.engfracmech.2007.02.012.

[4] A. Beheshti and M.M. Khonsari. 2011. On the prediction of fatigue crack initiation in rolling/sliding contacts with provision for loading sequence effect, *Tribology Int.*, 44(12), 1620-1628. http://dx.doi.org/10.1016/j.triboint.2011.05.017.

[5] J.W. Ringsberg. 2001. Life prediction of rolling contact fatigue crack initiation, *Int. J. Fatigue*, 23(7), 575-586. http://dx.doi.org/10.1016/s0142-1123(01)00024-x.

[6] R. Heyder and M. Brehmer. 2014. *Empirical studies of head check propagation on the DB network*, Wear, 314(1-2), 36-43. http://dx.doi.org/10.1016/j.wear.2013.11.035.

[7] W.J. Wang, H.M. Guo, X. Du, J. Guo and Q.Y. Liu. 2013. Investigation on the damage mechanism and prevention of heavy-haul railway rail, *Engg. Failure Analysis*, 35, 206-218. http://dx.doi.org/10.1016/j.engfailanal.2013.01.033.

[8] H. Choi, D. Lee and J. Lee. 2013. *Optimization of a railway wheel profile to minimize flange wear and surface fatigue*, Wear, 300(1-2), 225-233. http://dx.doi.org/10.1016/j.wear.2013.02.009.

[9] M. Rajasekaran. 2016. A new minimal part breakup body-in-white design approach and optimal material map strength assessment, *J. Teknologi*, 78(7), 17-22.

[10] P. Christodoulou, A. Kermanidis and G. Haidemenopoulos. 2016. Fatigue and fracture behaviour of Pearlitic grade 900A steel used in railway applications, *Theoretical and Applied Fracture Mechanics*, 83, 51-59. http://dx.doi.org/10.1016/j.tafmec.2015.12.017.